Giant boulders and Last Interglacial storm intensity in the North Atlantic

Alessio Rovere[a,b,c,1], Elisa Casella[b], Daniel L. Harris[a,b,d], Thomas Lorscheid[a,b], Napayalage A. K. Nandasena[e], Blake Dyer[c], Michael R. Sandstrom[c], Paolo Stocchi[f,g], William J. D'Andrea[c], and Maureen E. Raymo[c,1]

[a]Center for Marine Environmental Sciences (MARUM), University of Bremen, D-28359 Bremen, Germany; [b]Leibniz Centre for Tropical Marine Research (ZMT), D-28359 Bremen, Germany; [c]Lamont-Doherty Earth Observatory, Columbia University, Palisades, NY 10964; [d]School of Earth and Environmental Sciences, The University of Queensland, Brisbane, QLD 4072, Australia; [e]Department of Civil and Environmental Engineering, University of Auckland, Auckland 1010, New Zealand; [f]Department of Coastal Systems, Royal Netherlands Institute for Sea Research (NIOZ), 1790 AB Den Burg, Texel, The Netherlands; and [g]Utrecht University, 3512 JE Utrecht, The Netherlands

Contributed by Maureen E. Raymo, September 26, 2017 (sent for review July 12, 2017; reviewed by Max Engel and Robert E. Kopp)

As global climate warms and sea level rises, coastal areas will be subject to more frequent extreme flooding and hurricanes. Geologic evidence for extreme coastal storms during past warm periods has the potential to provide fundamental insights into their future intensity. Recent studies argue that during the Last Interglacial (MIS 5e, ∼128–116 ka) tropical and extratropical North Atlantic cyclones may have been more intense than at present, and may have produced waves larger than those observed historically. Such strong swells are inferred to have created a number of geologic features that can be observed today along the coastlines of Bermuda and the Bahamas. In this paper, we investigate the most iconic among these features: massive boulders atop a cliff in North Eleuthera, Bahamas. We combine geologic field surveys, wave models, and boulder transport equations to test the hypothesis that such boulders must have been emplaced by storms of greater-than-historical intensity. By contrast, our results suggest that with the higher relative sea level (RSL) estimated for the Bahamas during MIS 5e, boulders of this size could have been transported by waves generated by storms of historical intensity. Thus, while the megaboulders of Eleuthera cannot be used as geologic proof for past "superstorms," they do show that with rising sea levels, cliffs and coastal barriers will be subject to significantly greater erosional energy, even without changes in storm intensity.

Last Interglacial | Eemian | climate change | extreme waves | superstorms

Coastal areas are at risk from climate change and sea-level rise. The combined effect of storm surges, extreme tides, and extreme wave events could, in some areas, double the frequency of coastal flooding by 2050 (1). This is a growing global threat to coastal communities, infrastructure, and industries, and it is important to understand the extent to which extreme storms (such as tropical cyclones) will change in intensity and frequency under warmer climates and how this will affect our future coastlines.

Observational data (2) allow analysis of historical tropical cyclone frequency and intensity, while coupled ocean–atmosphere models (3) can be used to estimate the likelihood of changes to tropical cyclones as global climate warms (4–6). Based on one century of observational data, the Fifth Assessment Report of the Intergovernmental Panel on Climate Change (IPCC AR5) concluded that at the global scale there has been no statistically significant increase in tropical cyclone activity (7). However, they also concluded that it is "virtually certain that the frequency and intensity of the strongest tropical cyclones in the North Atlantic has increased since the 1970s" (2, 7, 8). At the same time, climate model projections (3) of future storm activity are ascribed "low confidence" with respect to basin-scale projections of changes in the intensity and frequency of tropical cyclones (9).

Beyond the study of historical observations and model projections, it is possible to investigate hurricane intensity during past periods of warmer climate to provide sensitivity bounds for future predictions. A similar approach was recently used to calibrate models of future Antarctic ice melting against mid-Pliocene and Last Interglacial (LIG) sea-level estimates (10). During the LIG (also referred to as the Eemian or MIS 5e, ∼128–116 ka), atmospheric CO_2 concentrations were similar to preindustrial levels (280–290 ppm) (11, 12). While LIG sea-surface temperatures in tropical areas were slightly cooler than preindustrial, in extratropical areas they were, on average, 1.1–1.3 °C warmer than preindustrial (12). As a result of this modestly warmer climate, polar ice sheets were smaller and global mean sea levels are estimated to have been between 6 and 9 m higher than present (13, 14).

A recent study (15) proposed that, during the LIG, the shutdown of the Atlantic Meridional Overturning Circulation increased the equator-to-pole temperature gradient, resulting in enhanced wind energy over the North Atlantic. The increased wind strength was hypothesized to have generated storms of greater intensity than those historically observed, i.e., "superstorms" (15, 16), that directed large ocean swells toward the eastern margins of the Bahamas and Bermuda. Three lines of geologic evidence have been invoked to support the inference of LIG superstorms in the North Atlantic: (*i*) massive cliff-top boulders on the island of Eleuthera, Bahamas that are bigger than any boulders known to have been moved or emplaced

Significance

The Last Interglacial was the last period of the Earth's history when climate was warmer than preindustrial, with higher polar temperatures and higher sea levels. Based on geologic evidence in Bermuda and the Bahamas, studies suggest that during this period the North Atlantic was characterized by "superstorms" more intense than any observed historically. Here we present data and models showing that, under conditions of higher sea level, historically observed hurricanes can explain geologic features previously interpreted as evidence for more intense Last Interglacial storm activity. Our results suggest that, even without an increase in the intensity of extreme storms, cliffs and coastal barriers will be subject to significantly higher wave-induced energies under even modestly higher sea levels.

Author contributions: A.R., D.L.H., and M.E.R. designed research; A.R., E.C., T.L., B.D., M.R.S., W.J.D., and M.E.R. performed research; A.R., E.C., D.L.H., T.L., N.A.K.N., M.R.S., P.S., and M.E.R. analyzed data; D.L.H., T.L., N.A.K.N., P.S., and W.J.D. wrote sections of the SI Appendix and manuscript; B.D. contributed to sections of the paper and SI Appendix; M.R.S. wrote sections of the SI Appendix and manuscript; and A.R., E.C., and M.E.R. wrote the paper.

Reviewers: M.E., Universität zu Köln; and R.E.K., Rutgers University.

Conflict of interest statement: A.R. and R.E.K. are coauthors on a 2016 multiauthor review paper. This was not a research collaboration.

Data deposition: The data reported in this paper have been deposited in the PANGEA database (https://doi.pangaea.de/10.1594/PANGAEA.880687).

[1]To whom correspondence may be addressed. Email: arovere@marum.de or raymo@ldeo.columbia.edu.

This article contains supporting information online at www.pnas.org/lookup/suppl/doi:10.1073/pnas.1712433114/-/DCSupplemental.

during the Holocene in the Bahamas (17); (*ii*) shore-parallel deposits throughout the Bahamas and in Bermuda, hypothesized to have been deposited by storm surges (18, 19); and (*iii*) westward-pointing "chevron-shaped" ridges observed throughout the Bahamas and extending kilometers inland, proposed to represent massive storm surge overwash deposits (19).

The attribution of this geological evidence to superstorms has been controversial for years (20–25). Here we examine the most widely cited line of evidence: the massive cliff-top boulders of Eleuthera, Bahamas. Seven massive boulders (weighing hundreds of tons, *SI Appendix*) lie atop and behind an ∼15-m-high cliff on North Eleuthera, at a locality known as Glass Window Bridge (Fig. 1 *A* and *B*). Two of the biggest boulders are known by the local names "Cow" and "Bull" (Fig. 1*C*). Based on field observations, estimates of boulder masses, and simple wave-flow calculations, Hearty (17) proposed that these boulders were deposited by storm waves of "considerably greater magnitude than storms during the Holocene" (15–17, 19). The same conclusion is restated in a recent review on the geologic superstorms evidence (16).

Here we address the following question: Could these massive boulders have been transported from the cliff face to their modern positions during the LIG by waves generated by storms of historical magnitude? To answer this question we integrate geologic field surveys with hydrodynamic and boulder transport models (see *Methods* and *SI Appendix* for details) to determine if superstorms are necessary to move boulders of this size.

Results

We propagate the waves generated by three historical storms toward the Glass Window Bridge cliffs using a set of 2D and 1D wave and hydrodynamic models (26, 27). We reproduce the waves generated by the Perfect Storm (1991) (Fig. 2 *A*, *D*, *G*, and *J*), Hurricane Andrew (1992) (Fig. 2 *B*, *E*, *H*, and *K*), and Hurricane Sandy (2012) (Fig. 2 *C*, *F*, *I*, and *L*). These swells produced some of the highest-amplitude and longest-period waves to hit Eleuthera in instrumental times, but each storm also differed substantially with respect to its track, intensity, and development (see tracks in Fig. 1*A* and nearshore significant wave heights in Fig. 2 *A*–*C*).

To account for the higher local relative sea level (RSL) during the LIG, we incrementally adjust RSL from today's value (0 m) up to +15 m in our wave models. This range was selected to encompass MIS 5e RSL estimates at Whale Point, ∼2 km north of Glass Window Bridge (28). Field data and relative sea level predictions from glacial isostatic adjustment (GIA) models (29, 30) suggest that LIG RSL could have been between ∼5 and ∼15 m above present at this location (Fig. 3*A*) (see *SI Appendix* for details on RSL indicators in the area and GIA models).

From our hydrodynamic models, we calculate the wave-induced flow velocities impacting the Glass Window Bridge cliffs under different storm and RSL scenarios (see *Methods* and Fig. 3*C* and *SI Appendix* for detailed results). Because flow velocity is directly related to the energy a wave exerts on a solid boundary, we use this output to evaluate whether the historical storms generated flow velocities sufficient to transport the Cow and Bull boulders.

Using drone and field photographs analyzed with Structure-from-Motion, we built a 3D model of the boulders at Glass Window Bridge (Fig. 3*E*) and from this we estimate that the Cow and Bull have volumes of 186 and 449 m^3, respectively. Using density estimates from rock samples (*Methods* and *SI Appendix*), we calculate their masses as 383 (Cow) and 925 tons (Bull). Using these dimensions and a set of equations determined by empirical evidence and principles of physics and fluid flow (31), we then calculate the minimum flow required to lift or roll the boulders from just below the edge of a cliff onto the cliff top. We calculate that the Cow boulder can be lifted or rolled when the flow velocity generated by

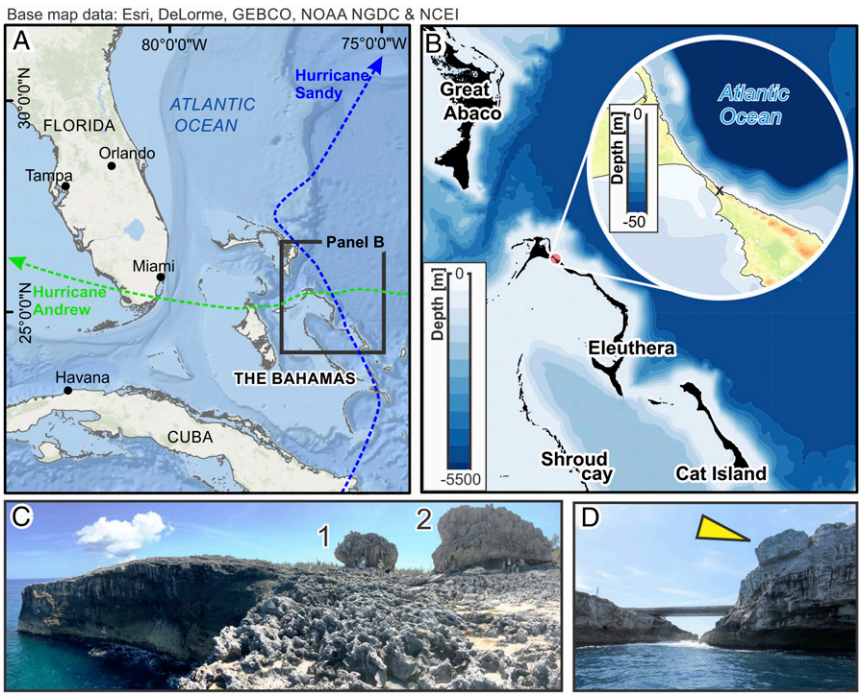

Fig. 1. Geographic location of Glass Window Bridge and the Cow and Bull boulders, North Eleuthera, Bahamas. (*A*) Location of the study area in the context of the Western Atlantic Ocean. The blue and green dashed lines represent, respectively, the tracks of Hurricane Sandy (2012) and Hurricane Andrew (1992) (tracking data from NOAA National Hurricane Center). The third storm modeled in this study (Perfect Storm, 1991) originated further north, offshore Nova Scotia. (*B*) Location of Eleuthera island. The map *Inset* shows the topography and bathymetry of the Glass Window Bridge area. The black cross corresponds to the location of the Cow and Bull boulders. (*C*) The Cow (1) and Bull (2) boulders seen from the top of the Glass Window Bridge cliff, looking toward southeast. Note people near the boulders for scale. Photo courtesy of W.J.D. (*D*) The yellow triangle indicates a cliff-edge boulder near the Glass Window Bridge. This boulder's major axis is ∼5 m. Photo courtesy of E.C.

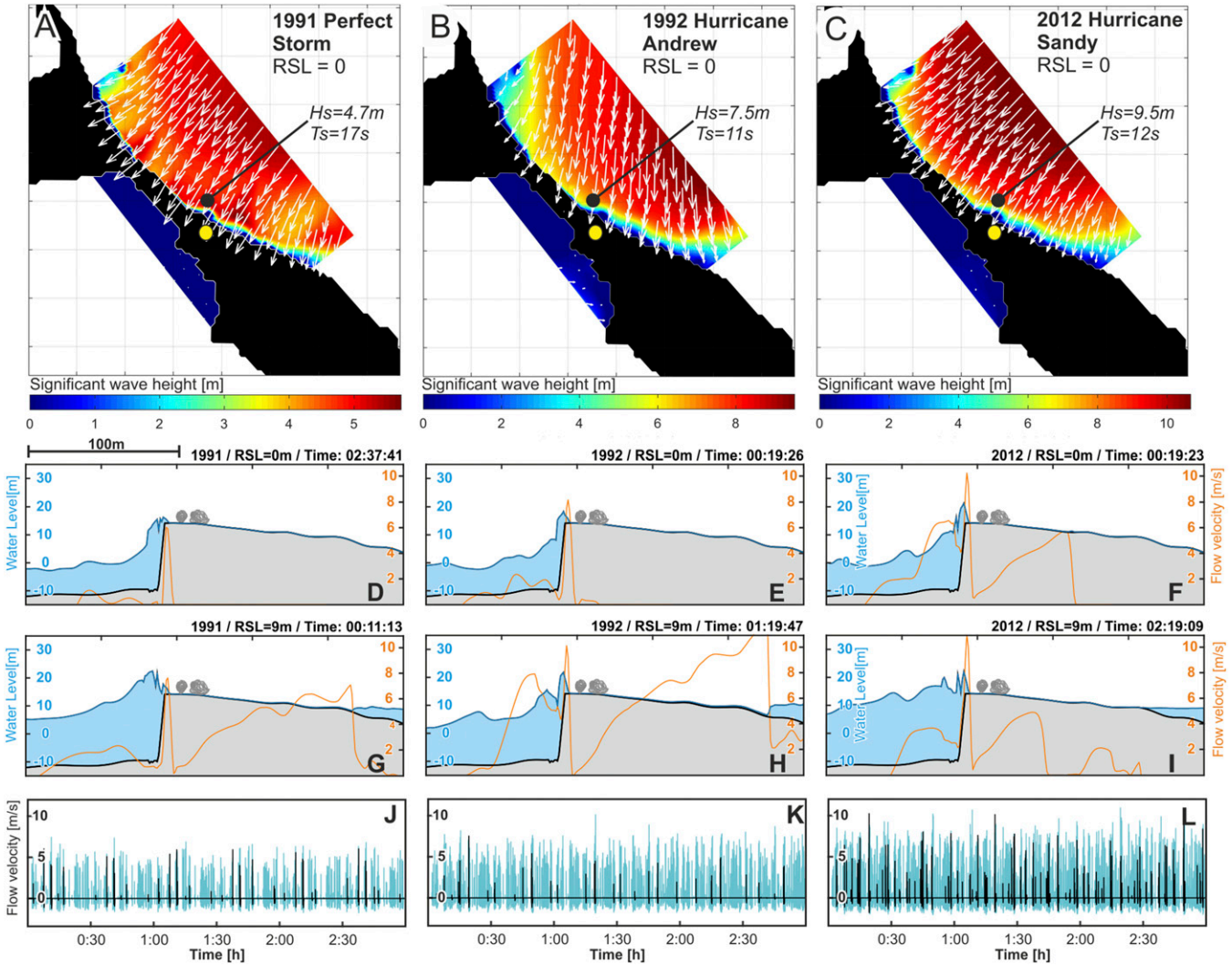

Fig. 2. Results of 1D and 2D wave and hydrodynamic models. (*A–C*) Wave height calculated in proximity of Glass Window Bridge (2D wave model SWAN) for the three storms modeled in this study. The white arrows represent the peak wave direction; the yellow dots shows the location of the Cow and Bull boulders; the black dots show the location where *Hs* and *Ts* (respectively, the significant wave height and period at RSL = 0 m) have been extracted from the 2D models and used in the 1D simulations (see *SI Appendix* for details). (*D–F*) Water level (blue scale on the left) and flow velocity (orange scale on the right) calculated at RSL = 0 m (1D XBeach model) at the Cow and Bull cliffs for the three swells modeled in this study. The "Time" in the upper right corner of each panel indicates the time elapsed since the beginning of the 3-h simulation at which the wave and flow shown in each panel have been extracted. (*G–I*) Same as *D–F*, but with RSL = 9 m. (*J–L*) Flow velocity field at the cliff edge calculated by 3-h run of the 1D XBeach model. Black lines represent RSL = 0 m; cyan lines represent RSL = 9 m.

waves against the Glass Window Bridge cliffs reaches at least 9.1 (lifting) or 9.3 (rolling) m/s. The larger Bull boulder can be lifted at a flow velocity of 10.8 m/s and can be rolled at flow velocities above 11.2 m/s (see *SI Appendix* for details). Overall, our results show that when the critical flow velocity of 10.8 m/s is surpassed, both boulders can be moved from the cliff edge across the cliff top.

Putting this all together, our results show that it is not necessary to invoke LIG superstorms to explain the current position of the Eleuthera Cow and Bull boulders. At the minimum assumed LIG sea level (~5 m), or even slightly lower (3.5 m above present, Fig. 3*A*) waves generated by an event analogous to Hurricane Sandy (2012) could have produced flows great enough to transport the Cow and Bull boulders from the cliff edge to their modern position (Fig. 3 *A* and *C*). Waves from Hurricane Andrew (1992) could have moved both boulders at RSL = 12.5 m, which is still in the range of possible LIG sea levels in the area. The waves modeled for the Perfect Storm (1991) can hardly move even the smaller boulder (Cow) in any RSL scenario.

Discussion

Our model results show that significantly greater flow velocities are reached at the cliff edge under higher sea levels, and also that the frequency of high flows hitting the cliff lip is much higher (compare black and cyan lines in Fig. 2 *J–L*). Furthermore, at higher RSLs, the wave flow over the top of the cliff would likely be great enough (above 10 m/s and flowing downward, orange lines in Figs. 2 *G–I* and 3*D*) to transport boulders similar in size to the Cow and Bull across the Glass Window Bridge isthmus toward the lagoon side of the island, consistent with the positions of five additional large boulders (17).

Based on controversial amino acid racemization dates, it was proposed that the Cow and Bull boulders were lifted from the base of the cliff face and transported up and over the cliff top (17) by waves. This would require a larger vertical displacement (~15 m) than we have considered in our model, and would probably require much greater wave-flow velocities. While such a mode of vertical transport has been seldom, if ever, reported for

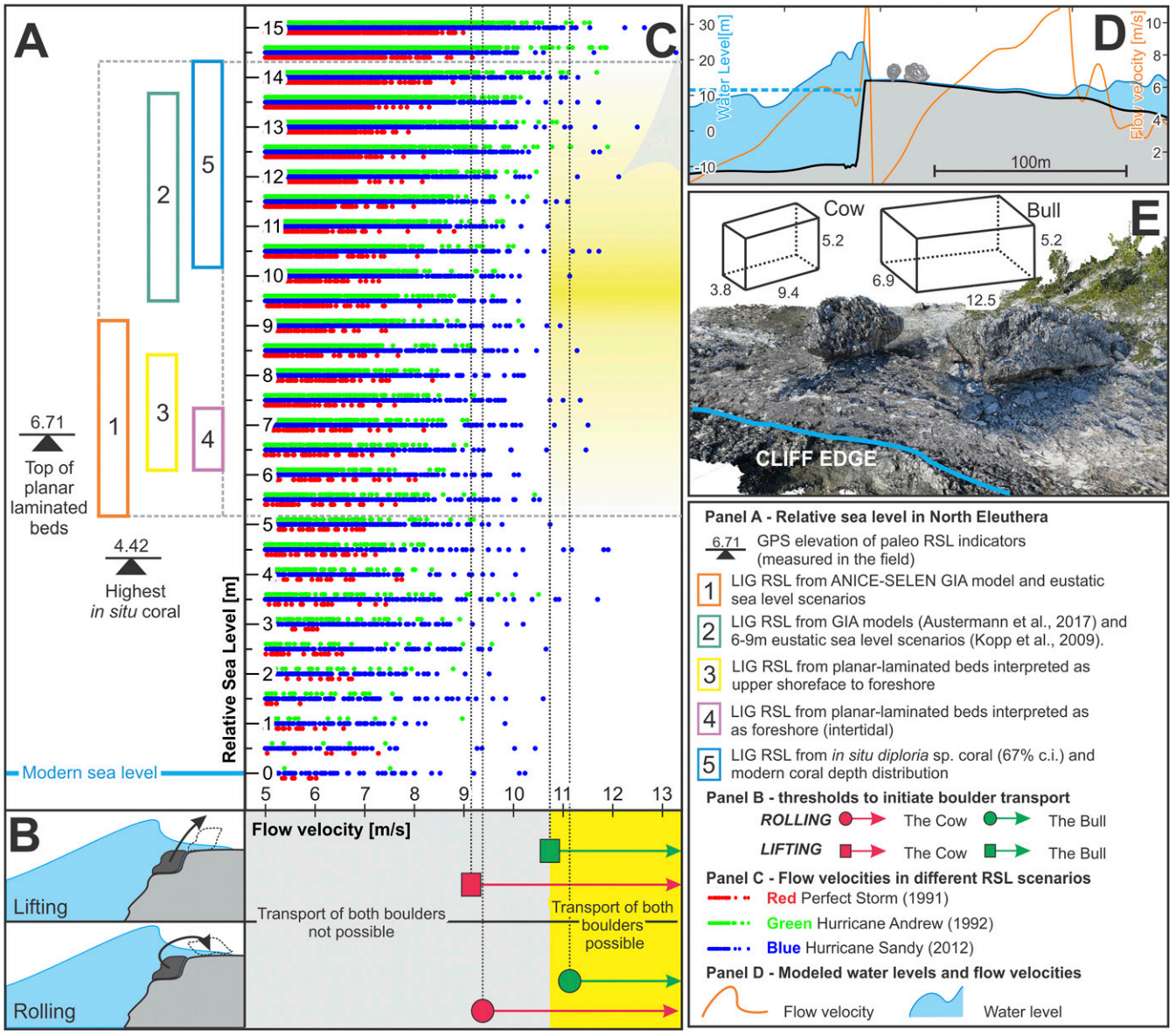

Fig. 3. Comparison between RSL field data, modeled flow velocities, and threshold flow velocities needed to transport the Cow and Bull from the cliff edge. (*A*) Compilation of RSL estimates for Whale Point, North Eleuthera (28) (see *SI Appendix* for detailed results). (*B*) Results of the calibrated boulder transport equations for the Cow and Bull boulders under different transport modes (lifting or rolling). (*C*) Modeled wave-generated flow velocities against the Glass Window Bridge cliff during the peak of each event considered in this study under different RSL scenarios. The yellow box highlights the most likely range of MIS 5e RSL and wave-flow velocities as shown in *A* and *B*, respectively. (*D*) Results of 1D nonhydrostatic XBeach runs with RSL = 12.5 m. (*E*) Three-dimensional model of the Cow and Bull boulders with calculated dimensions (in meters).

modern and Holocene boulders, abundant examples of modern cliff-edge boulders being transported backward from the cliff lip by large storms (or tsunamis) are observed in Eleuthera, as well as at many other locations in the Caribbean and elsewhere (32–35). In close proximity to the Cow and Bull boulders, near the Glass Window Bridge cliffs, we identified at least one large boulder in cliff-edge position (Fig. 1*D*) and two smaller ones that were transported across the cliff top from the cliff edge by the waves of Hurricane Andrew (see *SI Appendix* for details).

The most likely transport scenario for the massive cliff-top boulders of Eleuthera is that, like the smaller modern boulders, they were lifted or rolled from the cliff edge to their current positions. The transport would have only required waves generated by storms of historical magnitude, in combination with higher Eemian sea level.

In light of these results, we suggest that the remaining geologic evidence for superstorms should also be reanalyzed using numerical and process-based approaches similar to those applied here. We also highlight that, given the large number of MIS 5e coastal deposits (e.g., boulder fields or beach ridges) identified worldwide (36), there is an unexplored potential to use coastal landforms to assess potential changes in the intensity of storms and swells during the LIG, beyond the often-reported records of Bermuda and the Bahamas.

Our results also show that the maximum flow velocity against the top of the Eleuthera cliffs, generated by waves from each of the three storms, is greater as sea level is increased in the model. Comparing the maximum flow calculated at each RSL to the maximum flow modeled at present RSL for each storm (Fig. 4), we calculate that ~90% of the maximum wave flows at higher

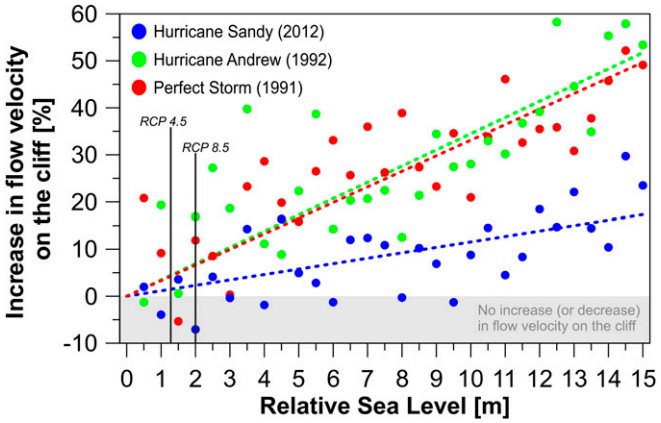

Fig. 4. Percent increase in maximum flow velocity against the Glass Window Bridge cliffs, Eleuthera, under conditions of higher sea levels for the three storms modeled in this study. Median global sea-level projections for 2200 according to Representative Concentration Pathways (RCP) 4.5 and 8.5 (42) are shown for reference. Dashed lines represent the linear regression of RSL vs. maximum flow velocity for each storm.

RSLs are greater than the maximum modeled at present sea level. As an example, under median sea-level projections for the year 2200 (see black lines in Fig. 4), the flow velocity against the Glass Window Bridge cliffs by a Category 5 Hurricane (such as Andrew) might increase by ∼15% with respect to present. Our results (Fig. 2 *J*–*L*) also suggest that these high flows are more frequent during a single storm event when sea level is higher than at present.

These results point to an important conclusion concerning the future: Even without an increase in the intensity of coastal storms, rising sea levels have the potential to cause significant increases in both the frequency of strong waves delivered during a given storm event as well as the magnitude of flow velocities (and hence wave-related energy) experienced by coastlines, coastal communities, and infrastructure. Even cliffs and hard coastal barriers such as the one studied here, barriers which are often considered the more resistant elements of our coastlines, will be subject to higher erosional energy with sea level only a few meters higher than today. Future research on coastal processes at higher sea level (37) will therefore be critical to efforts aimed at adapting to and mitigating global warming and its impact on the people that currently live within the coastal zone.

Methods

We use two independent workflows to calculate, respectively, the flow velocity generated by waves hitting the Glass Window Bridge cliffs under different sea-level scenarios and the flow velocity required to initiate the boulder transport from the cliff edge. The description of each method employed in this study is summarized in Fig. 5. In *SI Appendix* we report the full details on our methods as well as detailed results for each step in the workflows.

We mapped the topography and bathymetry of the Glass Window Bridge area using a differential GPS and a single-beam echosounder, respectively. We interpolated these data with large-scale datasets from SRTM (38) and GEBCO (39). We used photogrammetry and representative rock samples to calculate exact measurements of the external dimensions, volumes, and masses of the Cow and Bull boulders.

The bathymetric and topographic data were used as input to a modeling chain consisting of a 1D nonhydrostatic wave model (26) coupled with a 2D phase-averaged model (27). The 2D model was used to propagate offshore waves from the global model WaveWatch III (40, 41) toward the area of Glass Window Bridge, while the 1D model was used to propagate the waves toward the cliff and calculate the cliff-top flow velocities generated by each swell modeled in this study. We modeled three storm-swell scenarios driven by historical observations: the Perfect Storm (1991), Hurricane Andrew (1992), and Hurricane Sandy (2012). RSL was changed from 0 to 15 m above

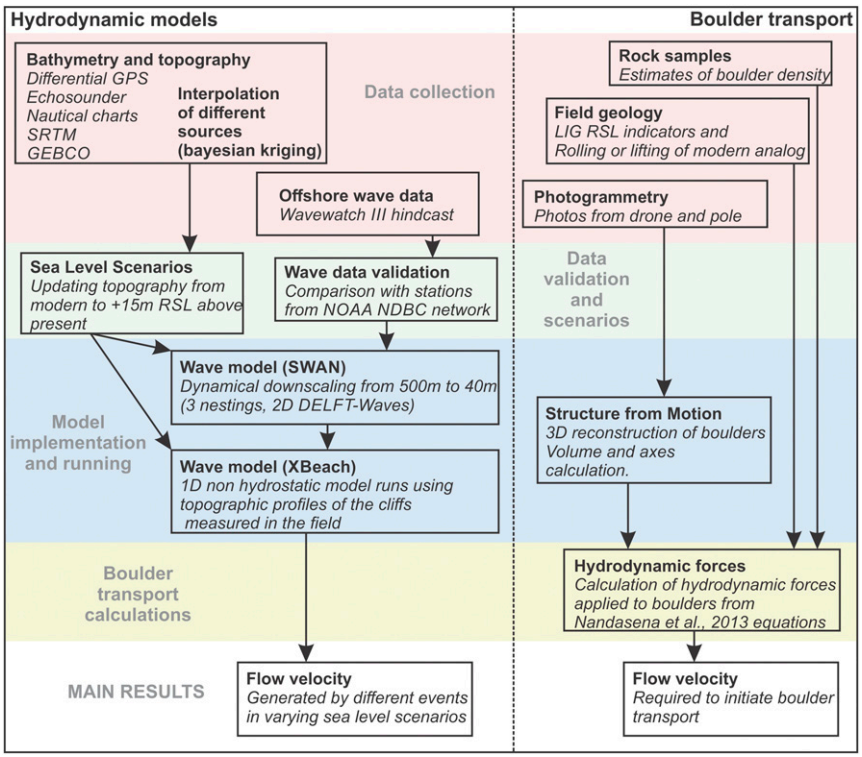

Fig. 5. Workflows used to model the flow velocities produced in different sea-level scenarios (*Left*) and to assess the minimum flow velocity required to move boulders (*Right*).

present sea level at intervals of 3 and 0.5 m for, respectively, 2D and 1D simulations.

To evaluate the threshold flow velocities needed to transport the boulders, we use the cliff-edge boulder transport equations of Nandasena et al. (31). These equations are sensitive to a number of variables, such as boulder shape, suspension load in the fluid, particle–particle interaction, bottom roughness, and a set of coefficients. In particular, they are most sensitive to the coefficient of lift that determines the lift force/moment needed to transport a boulder from the cliff edge. We used two smaller boulders (13 and 33 tons, respectively) that were deposited on the upper part of the Glass Window Bridge cliff by the waves of Hurricane Andrew to calculate the coefficient of lift for the carbonate rocks of the Eleuthera cliff. This value was determined to be between 2.006 and 2.775 (see *SI Appendix* for details). In *SI Appendix* we further discuss potential uncertainties related to our modeling approach, including 1D, 2D, and boulder transport model uncertainties and the possible influence of different paleo topography of Glass Window Bridge during the LIG.

To calculate the percentage of maximum flow increase at higher RSLs (Fig. 4), we used the following formula:

$$F_i^{\%} = \frac{\left(F_{\mathrm{RSL}}^{\max} - F_0^{\max}\right)}{F_0^{\max}} \times 100,$$

where $F_i^{\%}$ is the percentage increase in flow velocity, $F_{\mathrm{RSL}}^{\max}$ is the maximum flow for the specific swell at one RSL (from 1 to 15 m), and $F_0^{\max}$ is the maximum flow at RSL = 0 for the same swell. As also shown in Fig. 3*C*, $F_0^{\max}$ is 6.0 m/s for the Perfect Storm (1991), 7.5 m/s for Hurricane Andrew (1992), and 10.2 m/s for Hurricane Sandy (2012).

ACKNOWLEDGMENTS. We acknowledge P. J. Hearty and J. Hansen for discussions on LIG "superstorms." We acknowledge useful discussions during the workshops of Project 1603P (Modelling Paleo Processes, International Union for Quaternary Sciences, INQUA) and of the Paleo Constraints on Sea Level Rise (PALSEA) working group (Past Global Changes, PAGES/INQUA). Sarah Dendy and Alexander Janßen are acknowledged for help in the data analysis process. This research has been done under the permits issued by the Bahamas Environment, Science & Technology Commission [G-258] and the Bahamas Civil Aviation Authority (BCAA). We thank the staff at the Gerace Research Centre (San Salvador Island, The Bahamas) for logistical support for this research, the BCAA staff for assistance with aerial permits applications, and the staff at the Eleuthera Tourist Office for information on modern analog boulders. Boundary conditions and topography used in this study were extracted from datasets by the National Oceanic and Atmospheric Administration (NOAA), the US Geological Survey (USGS), the National Aeronautics and Space Administration (NASA), the Australian Bureau of Meteorology, the Commonwealth Scientific and Industrial Research Organisation (CSIRO), and the British Oceanographic Data Centre (BODC). The map in Fig. 1A was created using Esri ArcGIS basemaps and software (ArcMap). This research was financially supported by the Institutional Strategy of the University of Bremen, funded by the German Excellence Initiative (ABPZuK-03/2014); the Leibniz Centre for Tropical Marine Research (ZMT); National Science Foundation (NSF) Grant OCE-1202632 "PLIOMAX" and NSF GRFP Grant DGE-11-44155; and the World Surf League PURE through a grant from the Center for Climate and Life at the Lamont-Doherty Earth Observatory of Columbia University.

1. Vitousek S, et al. (2017) Doubling of coastal flooding frequency within decades due to sea-level rise. *Sci Rep* 7:1399.
2. Kossin JP, Knapp KR, Vimont DJ, Murnane RJ, Harper BA (2007) A globally consistent reanalysis of hurricane variability and trends. *Geophys Res Lett* 34:L04815.
3. Bender MA, et al. (2010) Modeled Impact of Anthropogenic Warming on the Frequency of Intense Atlantic Hurricanes. *Science* 327:454–458.
4. Oouchi K, et al. (2006) Tropical cyclone climatology in a global-warming climate as simulated in a 20 km-mesh global atmospheric model: Frequency and wind intensity analyses. *J Meteorol Soc Japan Ser II* 84:259–276.
5. Walsh KJE, Nguyen K-C, McGregor JL (2004) Fine-resolution regional climate model simulations of the impact of climate change on tropical cyclones near Australia. *Clim Dyn* 22:47–56.
6. Knutson TR, Tuleya RE (2004) Impact of CO2-induced warming on simulated hurricane intensity and precipitation: Sensitivity to the choice of climate model and convective parameterization. *J Clim* 17:3477–3495.
7. Hartmann DL, et al. (2013) *Observations: Atmosphere and Surface. Climate Change 2013: The Physical Science Basis. Contribution of Working Group I to the Fifth Assessment Report of the Intergovernmental Panel on Climate Change*, eds Stocker TF, et al. (Cambridge Univ Press, Cambridge, UK), pp 159–254.
8. Elsner JB, Kossin JP, Jagger TH (2008) The increasing intensity of the strongest tropical cyclones. *Nature* 455:92–95.
9. Kirtman B, et al. (2013) *Near-term Climate Change: Projections and Predictability. Climate Change 2013: The Physical Science Basis. Contribution of Working Group I to the Fifth Assessment Report of the Intergovernmental Panel on Climate Change*, eds Stocker TF, et al. (Cambridge Univ Press, Cambridge, UK), pp 953–1028.
10. DeConto RM, Pollard D (2016) Contribution of Antarctica to past and future sea-level rise. *Nature* 531:591–597.
11. Lüthi D, et al. (2008) High-resolution carbon dioxide concentration record 650,000-800,000 years before present. *Nature* 453:379–382.
12. Hoffman JS, Clark PU, Parnell AC, He F (2017) Regional and global sea-surface temperatures during the last interglaciation. *Science* 355:276–279.
13. Kopp RE, Simons FJ, Mitrovica JX, Maloof AC, Oppenheimer M (2009) Probabilistic assessment of sea level during the last interglacial stage. *Nature* 462:863–867.
14. Dutton A, Lambeck K (2012) Ice volume and sea level during the last interglacial. *Science* 337:216–219.
15. Hansen J, et al. (2016) Ice melt, sea level rise and superstorms: Evidence from paleoclimate data, climate modeling, and modern observations that 2°C global warming could be dangerous. *Atmos Chem Phys* 16:3761–3812.
16. Hearty PJ, Tormey BR (2017) Sea-level change and super storms; geologic evidence from late last interglacial (MIS 5e) in Bahamas and Bermuda offers ominous prospects for a warming Earth. *Mar Geol* 390:347–365.
17. Hearty PJ (1997) Boulder deposits from large waves during the last interglaciation on North Eleuthera Island, Bahamas. *Quat Res* 48:326–338.
18. Hearty PJ (2002) Revision of the late Pleistocene stratigraphy of Bermuda. *Sediment Geol* 153:1–21.
19. Hearty PJ, Neumann AC, Kaufman DS (1998) Chevron ridges and runup deposits in the Bahamas from storms late in oxygen-isotope substage 5e. *Quat Res* 50:309–322.
20. Hearty PJ, Tormey BR, Neumann AC (2002) Discussion of "Palaeoclimatic significance of co-occurring wind- and water-induced sedimentary structures in the last-interglacial coastal deposits from Bermuda and the Bahamas" (Kindler and Strasser, 2000, Sedimentary Geology, 131, 1-7). *Sediment Geol* 147:429–435.
21. Bain RJ, Kindler P (1994) Irregular fenestrae in Bahamian eolianites: A rainstorm-induced origin. *J Sediment Res* 64A:140–146.
22. Kindler P, Strasser A (2000) Palaeoclimatic significance of co-occurring wind- and water- induced sedimentary structures in the last-interglacial coastal deposits from Bermuda and the Bahamas. *Sediment Geol* 131:1–7.
23. Bourgeois J, Weiss R (2009) "Chevrons" are not mega-tsunami deposits—A sedimentologic assessment. *Geology* 37:403–406.
24. Mylroie JE (2008) Late Quaternary sea-level position: Evidence from Bahamian carbonate deposition and dissolution cycles. *Quat Int* 183:61–75.
25. Engel M, Kindler P, Godefroid F (2015) Speculations on superstorms – Interactive comment on "Ice melt, sea level rise and superstorms: Evidence from paleoclimate data, climate modeling, and modern observations that 2 ◦C global warming is highly dangerous" by J. Hansen et al. *Atmos Chem Phys Discuss* 15:C6270–C6281.
26. Roelvink D, et al. (2010) XBeach model description and manual (Version 6) (UNESCO-IHE Institute for Water Education, Deltares and Delft University of Technology, Delft, The Netherlands). Available at https://oss.deltares.nl/web/xbeach/. Accessed August 10, 2017.
27. Booij N, Ris RC, Holthuijsen LH (1999) A third-generation wave model for coastal regions: 1. Model description and validation. *J Geophys Res* 104:7649–7666.
28. Hearty PJ (1998) The geology of Eleuthera Island, Bahamas: A Rosetta stone of Quaternary stratigraphy and sea-level history. *Quat Sci Rev* 17:333–355.
29. De Boer B, Stocchi P, Van De Wal R, others (2014) A fully coupled 3-D ice-sheet-sea-level model: Algorithm and applications. *Geosci Model Dev* 7:2141–2156.
30. Austermann J, Mitrovica JX, Huybers P, Rovere A (2017) Detection of a dynamic topography signal in last interglacial sea-level records. *Sci Adv* 3:e1700457.
31. Nandasena NAK, Tanaka N, Sasaki Y, Osada M (2013) Boulder transport by the 2011 Great East Japan tsunami: Comprehensive field observations and whither model predictions? *Mar Geol* 346:292–309.
32. Etienne S, Paris R (2010) Boulder accumulations related to storms on the south coast of the Reykjanes Peninsula (Iceland). *Geomorphology* 114:55–70.
33. Williams DM, Hall AM (2004) Cliff-top megaclast deposits of Ireland, a record of extreme waves in the North Atlantic—storms or tsunamis? *Mar Geol* 206:101–117.
34. Cox R, Zentner DB, Kirchner BJ, Cook MS (2012) Boulder ridges on the Aran Islands (Ireland): Recent movements caused by storm waves, not tsunamis. *J Geol* 120:249–272.
35. Engel M, Oetjen J, May SM, Brückner H (2016) Tsunami deposits of the Caribbean – Towards an improved coastal hazard assessment. *Earth Sci Rev* 163:260–296.
36. Pedoja K, et al. (2014) Coastal staircase sequences reflecting sea-level oscillations and tectonic uplift during the Quaternary and Neogene. *Earth Sci Rev* 132:13–38.
37. Enríquez AR, Marcos M, Álvarez-Ellacuría A, Orfila A, Gomis D (2016) Changes in beach shoreline due to sea level rise and waves under climate change scenarios: Application to the Balearic Islands (Western Mediterranean). *Nat Hazards Earth Syst Sci Discuss* 25:1–25.
38. Farr TG, et al. (2007) The shuttle radar topography mission. *Rev Geophys* 45:RG2004.
39. GEBCO (2014) The GEBCO_2014 Grid, Version 20150318. Available at www.gebco.net. Accessed August 10, 2017.
40. The WAVEWATCH III Development Group (WW3DG) (2016) User manual and system documentation of WAVEWATCH III Version 5.16. - Tech. Note 329 (NOAA/NWS/NCEP/MMAB, College Park, MD).
41. Durrant T, Hemer M, Trenham C, Greenslade D (2013) Data from "CAWCR wave hindcast 1979-2010." v7. CSIRO. Data Collection. https://dx.doi.org/10.4225/08/523168703DCC5.
42. Kopp RE, et al. (2014) Probabilistic 21st and 22nd century sea-level projections at a global network of tide-gauge sites. *Earths Futur* 2:383–406.